

## Research Article

# Fluorinated Adenosine A<sub>2A</sub> Receptor Antagonists Inspired by Preladenant as Potential Cancer Immunotherapeutics

Gengyang Yuan,<sup>1</sup> Tanner C. Jenkins,<sup>1</sup> Christopher G. Patrick Jr.,<sup>1</sup> Phaethon Philbrook,<sup>2</sup> Olivia Sears,<sup>2</sup> Stephen Hatfield,<sup>2</sup> Michail Sitkovsky,<sup>2</sup> Neil Vasdev,<sup>3</sup> Steven H. Liang,<sup>3</sup> Mary Jo Ondrechen,<sup>1</sup> Michael P. Pollastri,<sup>1</sup> and Graham B. Jones<sup>1,4</sup>

<sup>1</sup>Department of Chemistry and Chemical Biology, Northeastern University, 360 Huntington Avenue, Boston, MA 02115, USA

<sup>2</sup>New England Tissue Protection Institute, Northeastern University, 360 Huntington Avenue, Boston, MA 02115, USA

<sup>3</sup>Gordon Center for Medical Imaging and Division of Nuclear Medicine and Molecular Imaging, Massachusetts General Hospital and Department of Radiology, Harvard Medical School, 55 Fruit St., Boston, MA 02114, USA

<sup>4</sup>Clinical and Translational Science Institute, Tufts University, 800 Washington Street, Boston, MA 02111, USA

Correspondence should be addressed to Graham B. Jones; [graham.jones@tufts.edu](mailto:graham.jones@tufts.edu)

Received 15 May 2017; Revised 31 August 2017; Accepted 13 September 2017; Published 19 October 2017

Academic Editor: Rosaria Volpini

Copyright © 2017 Gengyang Yuan et al. This is an open access article distributed under the Creative Commons Attribution License, which permits unrestricted use, distribution, and reproduction in any medium, provided the original work is properly cited.

Antagonism of the adenosine A<sub>2A</sub> receptor on T cells blocks the hypoxia-adenosinergic pathway to promote tumor rejection. Using an *in vivo* immunoassay based on the Concanavalin A mouse model, a series of A<sub>2A</sub> antagonists were studied and identified preladenant as a potent lead compound for development. Molecular modeling was employed to assist drug design and subsequent synthesis of analogs and those of tozadenant, including fluorinated polyethylene glycol PEGylated derivatives. The efficacy of the analogs was evaluated using two *in vitro* functional bioassays, and compound **29**, a fluorinated triethylene glycol derivative of preladenant, was confirmed as a potential immunotherapeutic agent.

## 1. Introduction

The adenosine receptors belong to the G protein-coupled receptor (GPCR) family including A<sub>1</sub>, A<sub>2A</sub>, A<sub>2B</sub>, and A<sub>3</sub>, four subtypes based on their different subcellular localization, signal transduction pathways, activation profiles, ligand binding profiles, and G protein binding preferences [1, 2]. Adenosine receptor coupling and subsequent dissociation with G<sub>i</sub> and G<sub>s</sub> proteins serve to regulate the level of adenylyl cyclase activity, thus controlling levels of intracellular cAMP, a second messenger known to trigger a complex sequence of cellular events [1–3]. As a consequence, A<sub>2A</sub>R has become a drug discovery target of increased interest, implicated in diseases such as neurodegenerative disorders (e.g., Parkinson's disease), cardiac ischemia, inflammation, and cancer [4–6]. After over a decade of effort applied to xanthine based A<sub>2A</sub>R antagonists, a derivative KW-6002 (istradefylline, **2**) was developed and approved in 2013 as an anti-Parkinson drug in Japan under the brand name

Nourias<sup>®</sup>. The molecule preladenant (**4**) completed Phase II clinical trials for Parkinson's disease but failed to show efficacy in subsequent Phase III trials. However, tozadenant (SYN115, **5a**) entered Phase III trials in 2015 for the same indication (Figure 1) [7–9].

Given the surge in interest in A<sub>2A</sub>R antagonists, we have focused effort on the immunomodulatory capacity of agents. We have previously demonstrated antagonism of the hypoxia-adenosinergic pathway, wherein hypoxia-driven accumulation of extracellular adenosine triggered immune suppression via A<sub>2A</sub>R activation on the surface of immune cells [10–15]. Subsequent A<sub>2A</sub>R antagonism by ZM241385 (**1**) led to delayed growth of CL8-1 melanoma in mice and increased levels of endogenous antitumor T cells [10–15]. Derivatization of xanthine **2** led to a PEG derivative (KW-PEG, **3**), which showed enhanced properties, including cAMP suppression and cytokine IFN- $\gamma$  restoration [16]. Spurred by these findings we were motivated to employ molecular modeling methods to design optimized derivatives

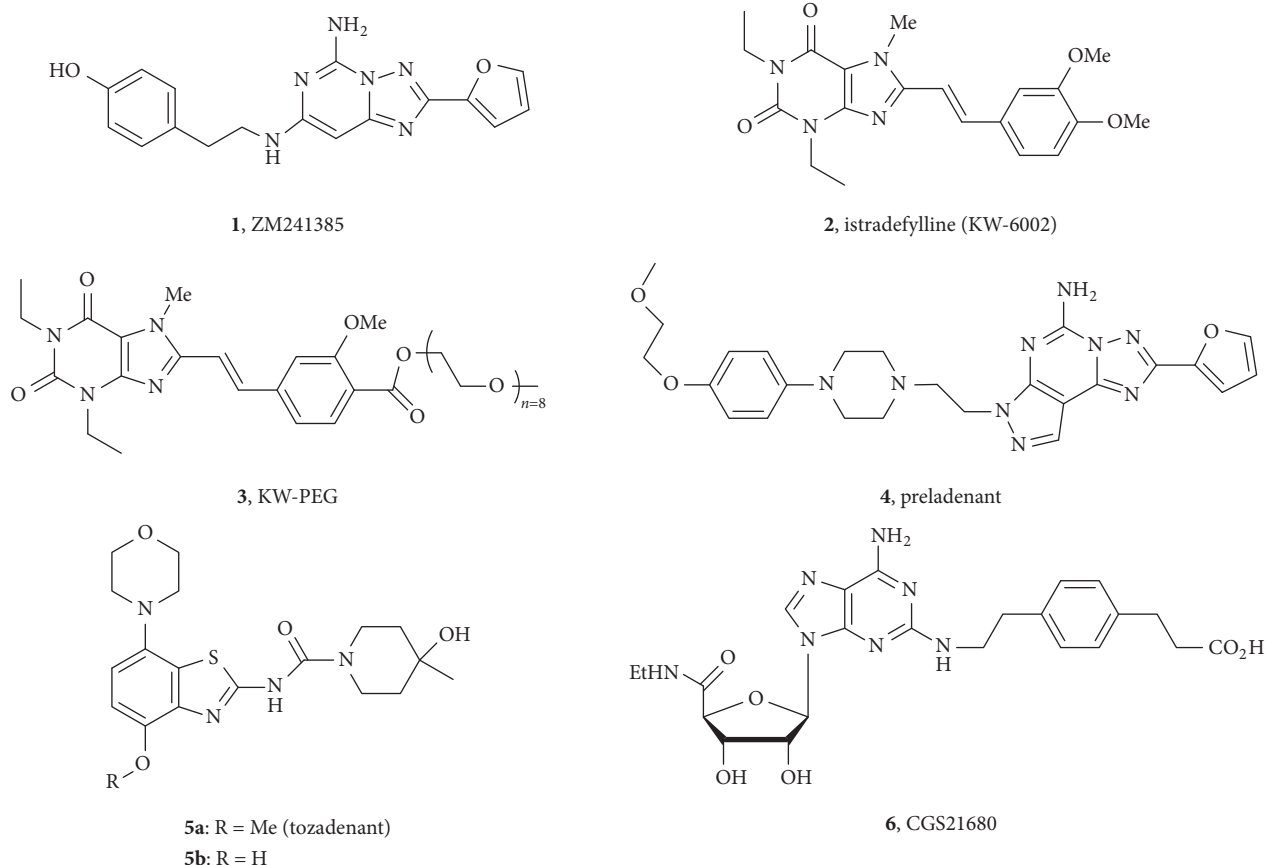


FIGURE 1: Structures of selected  $A_{2A}$ R antagonists 1–5a and  $A_{2A}$ R agonist CGS21680 (CGS, 6).



FIGURE 2: ConA-induced liver damage in C57BL/6 mice via CGS (6), 2, 3 and 4. Female C57BL/6 mice ( $n = 5$ ) were first injected with  $A_{2A}$ R agonist CGS (6,  $2 \text{ mg kg}^{-1}$ ),  $2 \text{ mg kg}^{-1}$  2, 3, and 4 separately, and then Con A ( $20 \text{ mg kg}^{-1}$ ). Con A-induced liver damage evaluated at 8 h.

(PEG) of other classes of  $A_{2A}$ R antagonists and to explore both their immunomodulatory capacity and potential to be converted to functional imaging agents.

## 2. Materials and Methods

To select lead compounds for immunotherapy application, an *in vivo* Concanavalin A (ConA)-induced liver damage assay was carried out in C57BL/6 mice through the pharmacological activation and deactivation of  $A_{2A}$ Rs [17]. A variety of compounds were screened including 2, 3, and 4 [10, 18, 19]. As shown in Figure 2, compound 4 imparted the most severe immune induced liver damage and was selected as a core structure for analog design. Fluorinated analogs were envisioned to potentially serve as leads to ultimately be labeled at the distal position with fluorine-18 ( $t_{1/2} = 109.8 \text{ min}$ ), for diagnostic imaging with positron

emission tomography (PET). A series of fluorinated PEG groups with increasing chain lengths were proposed for chemical modification to map the structure-activity relationship (SAR). Such modifications increase both hydrophilicity and molecular weight (MW), potentially to reduce blood-brain barrier (BBB) penetration as predicted by the central nervous system multiparameter optimization (MPO) score reported by Wager et al. [20].

To locate the ideal position for PEG attachment, molecular modeling was utilized based on our previously constructed homology model, which derived from the crystal structure of  $A_{2A}$ R in complex with 1 (PDB ID 3EML) and includes a resolved EL2 cap [16, 21, 22]. This technique employed Glide (Schrödinger, version 10.4, LLC, New York, NY, 2015) extra precision (XP) docking to gain insights into the ligand-protein binding interactions [23–26]. As shown in Figure 3(a), 4 almost occupies the entire binding

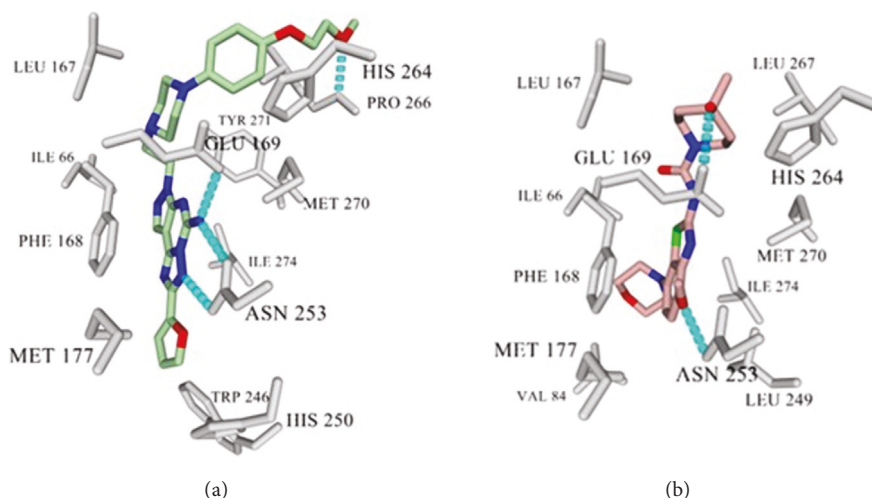


FIGURE 3: Glide XP docking results of **4** and **5a**. The interacting residues of A<sub>2A</sub>R are colored grey and the H-bond is represented as a dotted line. (a) **4** and (b) **5a** renderings from YASARA [39].

pocket of A<sub>2A</sub>R and shares similar key binding interactions as known ligand **1**. Noteworthy, the methoxyethyl ether group of **4** projects into the cytosolic solution and forms an additional H-bond with Pro266 at the solvent-exposed surface of the A<sub>2A</sub>R, connecting with the cytosolic solution. Similarly, the current clinical candidate **5a** also occupies a position near the edge of the A<sub>2A</sub>R binding pocket, where the piperidine quaternary alkyl group forms hydrophobic interactions with Leu267 and His264 and the tertiary alcohol group forms a hydrogen bond with Glu169 (Figure 3(b)) [27, 28]. It was thus suggested that introduction of hydrophilic and fluorinated PEG groups at the phenolic position of **4** and the piperidine component of **5a** would not impact key binding events of their core structures as the pendant groups would be capable of engaging in hydrogen bonds at the termini or in the case of their chains via hydrated networks. Accordingly, the octaethylene glycol monomethyl ether moiety, a tolerable substituent in prior studies on compound **2** [16] in conjunction with the phenyl-piperazine linker inherent in **4**, was introduced to **5a** and syntheses designed. In addition, synthesis of a demethylated version of the compound (**5b**) was planned, as such could be a useful intermediate for radiotracer synthesis (as either [<sup>11</sup>C]**5a** via a one-step [<sup>11</sup>C]CH<sub>3</sub>I methylation or a base-promoted coupling with an <sup>18</sup>F-labeled short alkyl chain) at this locus.

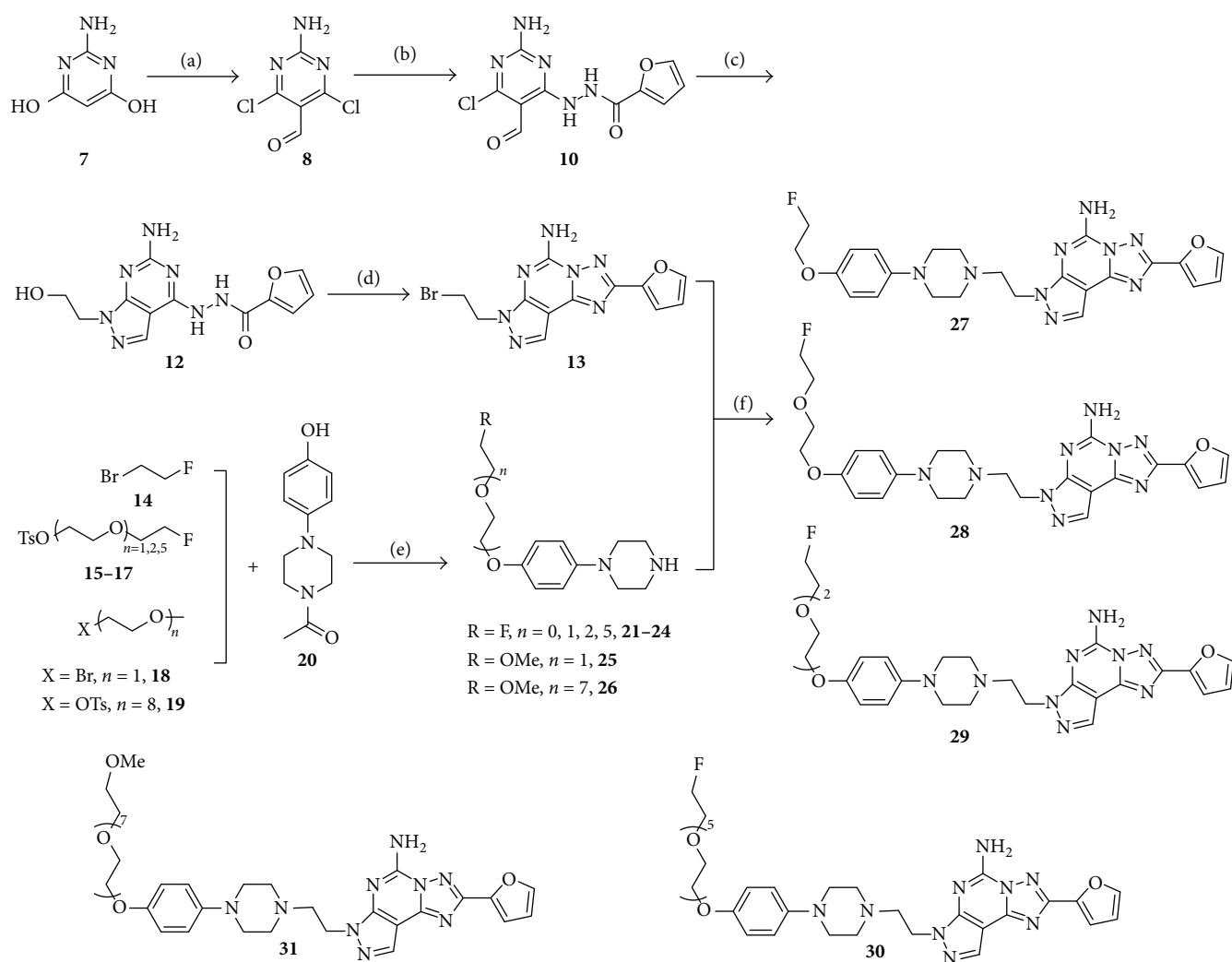
Synthesis of reference compounds **2** and **3** was performed using refinements of reported methods which produced superior yields independent of scale [16]. For example, use of a mild (AIBN/NBS promoted) route to the 8-substituted xanthine scaffold resulted in an improvement in yield from 22% to 56% for this key step (see experimental section) [29]. Compounds **4** and **5a** were synthesized based on modified literature methods (Scheme 1) [30–33], key intermediate **13** obtained from compound **7** via Vilsmeier-promoted halogenation and formylation, one-pot cascade condensation with 2-furoic acid hydrazine (**9**)

and 2-hydroxyethyl hydrazine (**11**), Dimroth rearrangement to effect triazole formation, and finally bromination with POCl<sub>3</sub>/ZnBr<sub>2</sub>. The piperazine components were prepared starting from either commercially available fragment **14** or fluorination/activation of the known mono- or ditosylated PEG chains (**15–19**) and subsequent coupling reaction with 1-(4-(4-hydroxyphenyl) piperazin-1-yl)ethan-1-one (**20**) and then deacetylation prior to the final coupling reaction with intermediate **13** to furnish **4** and the desired analogs **27–31** [30, 34].

Synthesis of **5a** is illustrated in Scheme 2. The bromide **32** was subjected to palladium-catalyzed coupling with morpholine (**33**), stannous nitro reduction, condensation with benzoyl isothiocyanate, bromine promoted formation of the benzothiazole ring, and installation of the piperidine ring through intermediate **38**. Preparation of analog **40** was achieved via coupling of **26** and **38** [31]. Direct demethylation of **5a** with BBr<sub>3</sub> did not lead to the desired product **5b** but instead led to decomposition and bromination of the tertiary alcohol [34]. Likewise, L-selectride promoted demethylation of **5a** led to very poor yield of product **5b** (5%) [35]. The sequence was finally realized when the phenyl carbamate protecting group of **38** was employed. With demethylation achieved, the phenyl carbamate protecting group (of **41**) was replaced by 4-methylpiperidin-4-ol **39** to afford desmethyl tozadenant, **5b**. Full details of all experimental procedures, bioassays, and molecular modeling are described in the Supplementary Material available online at <https://doi.org/10.1155/2017/4852537>.

### 3. Results and Discussion

Bioassay of compounds **27–31** and **40** and their parent compounds (**4** and **5a**) was conducted using two functional assays that evaluate A<sub>2A</sub>R binding-dependent signaling through A<sub>2A</sub>R on the surface of T cells [16]. The first assay screens



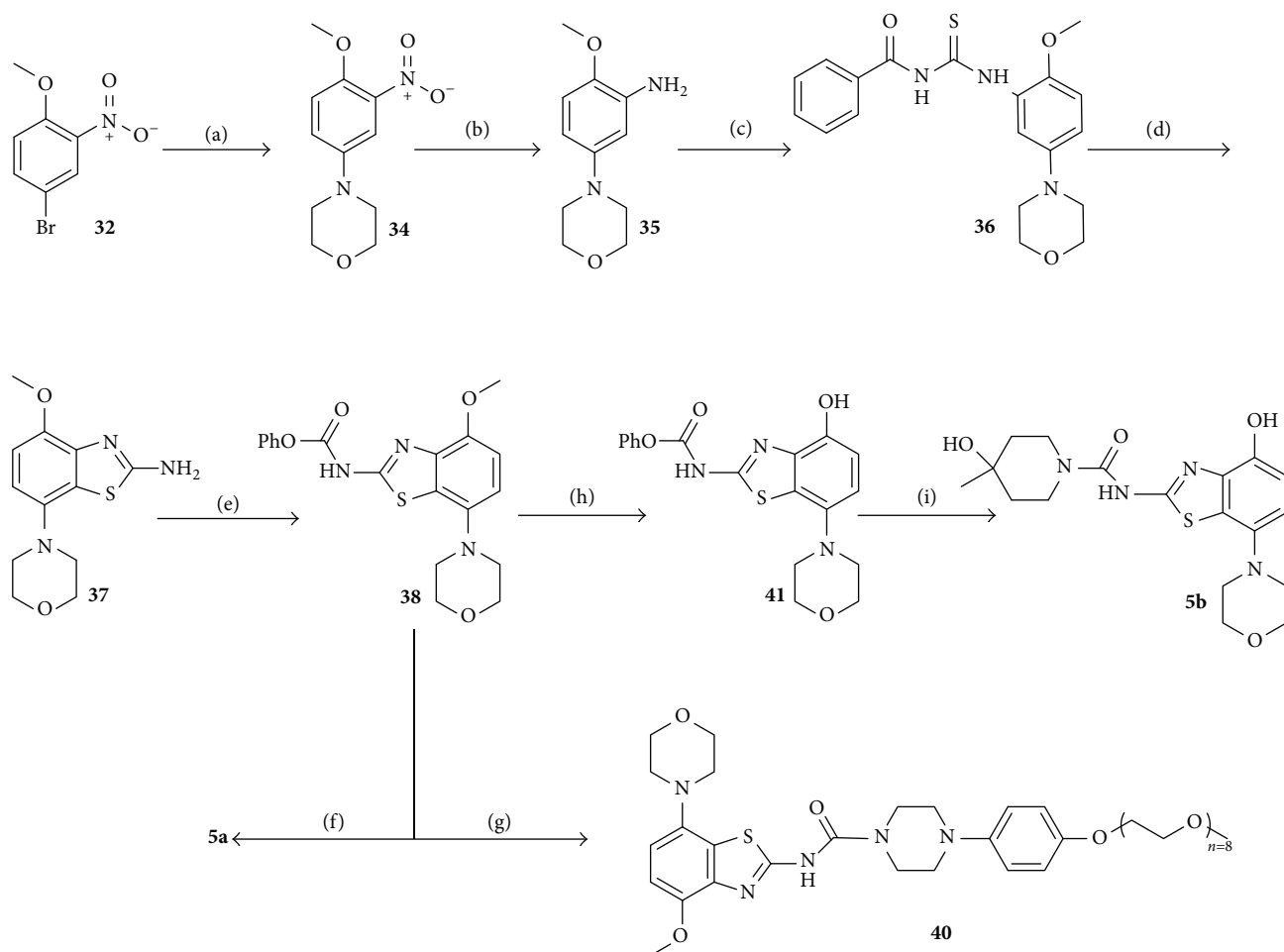
SCHEME 1: Synthesis of **4** and its PEGylated analogs. Conditions: (a)  $\text{POCl}_3$ , DMF, 78%; (b) 2-furoic acid hydrazide (**9**),  $\text{Na}_2\text{CO}_3$ , MeCN; (c) 2-hydroxyethyl hydrazine (**11**), 78% over 2 steps; (d)  $\text{POCl}_3$ ,  $\text{ZnBr}_2$ , 45%; (e) (i) NaH, DMF; (ii) 6 N HCl. 67% ( $n = 0$ , 21), 62% ( $n = 1$ , 22), 56% ( $n = 2$ , 23), 35% ( $n = 5$ , 24), 70% ( $n = 1$ , 25), 70% ( $n = 7$ , 26); (f) *N,N*-diisopropylethylamine (DIPEA), DMF, 52% ( $n = 0$ , 27), 47% ( $n = 1$ , 28), 33% ( $n = 2$ , 29), 25% ( $n = 5$ , 30), 55% ( $n = 1$ , 4), and 25% ( $n = 7$ , 31).

compounds on the basis of their extent of inhibition of  $\text{A}_{2\text{A}}\text{R}$ -induced intracellular cAMP accumulation in  $\text{A}_{2\text{A}}\text{R}$  expressing lymphocytes [36, 37]. The  $\text{A}_{2\text{A}}\text{R}$  agonist, CGS21680 (CGS, **6**), was used to activate  $\text{A}_{2\text{A}}\text{R}$ . As shown in Figure 4, all of the above compounds, except **40**, were able to prevent CGS-mediated signaling. Stronger antagonism was observed for the preladenant-based analogs **27–29** versus the previously evaluated compounds **2** and **3**. Further increments of the PEG chain length resulted in decreased antagonism (compounds **30** and **31**). Surprisingly, **5a** showed inferior antagonism to that of compounds **2** and **3**, and its derivative **40** exhibited no suppression of intracellular cAMP accumulation.

An evaluation of the positive hits in the cAMP assay (**27–29**) was carried out in silico by Glide docking to study their binding orientation in  $\text{A}_{2\text{A}}\text{R}$ . The docking results confirmed the initial assumption for such analog design (Figure 5), the core structures of **27–29** anchoring in similar

positions as **4**, forming identical key binding interactions with Asn253, Glu169, and Phe168. The installed PEG chains interact with the residues at the edge of  $\text{A}_{2\text{A}}\text{R}$  via hydrophobic and H-bonding interactions.

The second immunoassay assesses secretion of the cytokine IFN-gamma, since it is considered to be sensitive to the  $\text{A}_{2\text{A}}\text{R}$  signaling pathway [16]. In these assays, during T cell receptor (TCR) activation by the CD3 ligand, C57BL/6 mice splenocytes T cells are incubated with  $\text{A}_{2\text{A}}\text{R}$  agonist CGS to inhibit IFN-gamma secretion resulting from  $\text{A}_{2\text{A}}\text{R}$ -induced immunosuppression via intracellular cAMP. Effective  $\text{A}_{2\text{A}}\text{R}$  antagonists block the  $\text{A}_{2\text{A}}\text{R}$ -activated signal, thus restoring secretion of the cytokine to potentiate and prolong the immune response. Compounds **29**, **2**, **3**, and **4** were evaluated (Figure 6), and compound **29** showed similar capacity to that of **4**, both of which resulted in superior restoration of IFN-gamma secretion compared to either **2** or **3**.



SCHEME 2: Synthesis of **5a**, **5b**, and PEGylated analog **40**. Conditions: (a) morpholine (**33**),  $K_3PO_4$ , 2-biphenyl-dicyclohexylphosphine,  $Pd(OAc)_2$ , dimethoxyethane, 37%; (b) Sn powder, EtOH/con.HCl, 66%; (c) benzoyl isothiocyanate, acetone, 99%; (d) (i) NaOMe, MeOH; (ii)  $Br_2$ ,  $CHCl_3$ , 73%; (e) phenyl carbonochloridate, pyridine, dichloromethane, 94%; (f) 4-methylpiperidin-4-ol hydrochloride (**39**), DIPEA, THF,  $CHCl_3$ , 53%; (g) **26**, DIPEA, THF,  $CHCl_3$ , 28%; (h)  $BBr_3$ , dichloromethane, 52%; (i) (**39**), DIPEA, THF,  $CHCl_3$ , 62%.

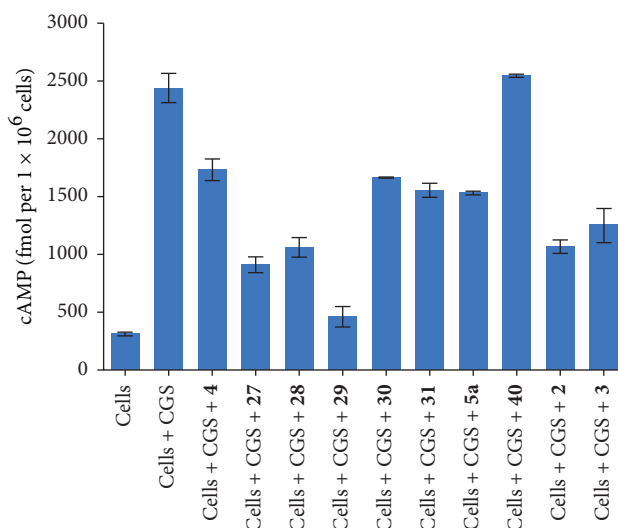


FIGURE 4: Intracellular cAMP levels in lymphocytes after incubation with vehicle,  $1 \mu M$  CGS, and  $1 \mu M$  CGS plus  $1 \mu M$  of compounds **4** (prelادenant), **27–31**, **5a** (tozadenant), **40**, **2** (KW-6002), and **3** (KW-PEG) are shown. The intracellular cAMP levels were determined 15 min following stimulation using quantitative cAMP ELISA and are expressed as fmol/ $10^6$  cells. Data shown represent mean  $\pm$  SEM of triplicate samples.



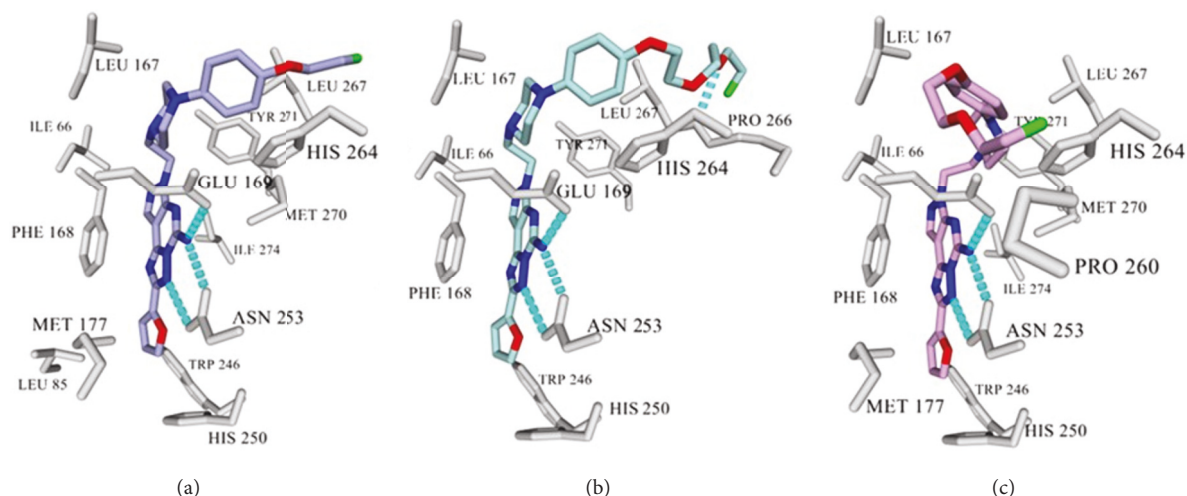


FIGURE 5: Docking results of **27–29** via Glide XP method. The interacting residues of A<sub>2A</sub>R are colored grey and the H-bond is represented as cyan dotted line. (a) Compound **27**. (b) Compound **28**. (c) Compound **29**. Rendered from YASARA [39].

TABLE 1: Physicochemical properties and docking results of compounds **27–29**.

Compound	Glide score	log $D_{7.4}$	Aqueous solubility ( $\mu$ M)	Human PPB (%)	HLM CLint ( $\mu$ L/min/mg)	Rat hepatocyte CLint ( $\mu$ L/min/10 <sup>6</sup> )
<b>27</b>	−12.2	2.8	74	99	16.5	29.9
<b>28</b>	−11.8	2.5	2	98.7	71.9	12.8
<b>29</b>	−12.3	2.3	10	98.3	66.1	72.9

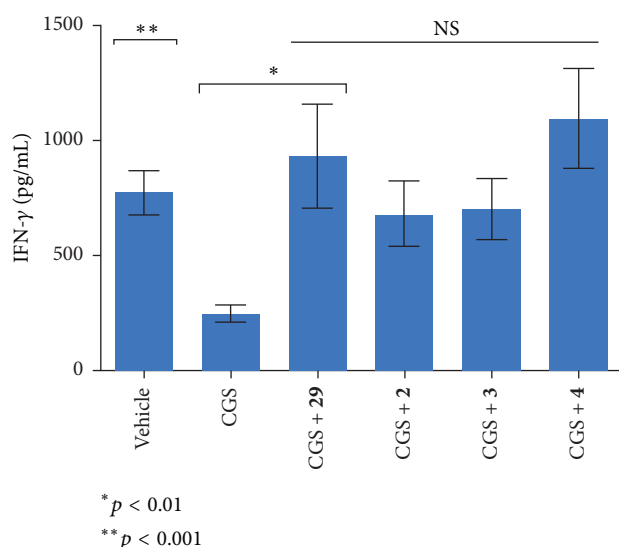


FIGURE 6: The IFN-gamma production by splenocytes after activation with 0.1  $\mu$ g/mL anti-CD3 and when treated with vehicle, 1  $\mu$ M CGS, and 1  $\mu$ M CGS plus 1  $\mu$ M compounds **29**, **2** (KW-6002), **3** (KW-PEG), and **4** (prelادنانت) separately is shown. The IFN-gamma levels were determined in the supernatant one day following stimulation using quantitative ELISA and are expressed as pg/mL. Data shown represent mean  $\pm$  SEM of triplicate samples.

Given the promising results in functional assays, the physicochemical properties of compound **29** and its homologs were determined, including its log  $D_{7.4}$ , aqueous solubility, human plasma protein binding (PPB), and metabolic stability [human liver microsome and rat hepatocyte clearance] as shown in Table 1. Broadly similar results were obtained, principle differences being enhanced aqueous solubility for **27**, whereas intrinsic clearance was superior for **29** in the rodent derived line and for **28** in the human cell line. Reduced clearance for **27** in turn may bode well for use in biodistribution studies [38].

## 4. Conclusions

In summary, we have designed and synthesized a family of PEGylated analogs of **4** and **5a** using molecular modeling techniques. Lead compound **29**, a fluorinated triethylene glycol derivative of prelادنانت, was identified, which shows promising results in two functional immunoassays and physicochemical assays. Future work will focus on detailed mechanistic studies on the mode of action of **29** and investigation of its use as a potential cancer immunotherapeutic agent.

## Conflicts of Interest

The authors report no conflicts of interest.

## Acknowledgments

This research was supported by Northeastern University and by grants from the National Institutes of Health (UL1TR001064 and CA111985-04) and National Science Foundation (MCB-1517290 and CHE-1305655). The authors are grateful to AstraZeneca for obtaining the measured physicochemical properties of **27–29** and Dr. Xi-Ping Huang for helpful discussions. Steven H. Liang is a recipient of NIH career development award from the National Institute on Drug Abuse (DA038000).

## References

- [1] K. A. Jacobson and Z. G. Gao, "Adenosine receptors as therapeutic targets," *Nature Reviews Drug Discovery*, vol. 5, pp. 247–264, 2006.
- [2] S. Moro, Z.-G. Gao, K. A. Jacobson, and G. Spalluto, "Progress in the pursuit of therapeutic adenosine receptor antagonists," *Medicinal Research Reviews*, vol. 26, no. 2, pp. 131–159, 2006.
- [3] M. Congreve, C. J. Langmead, J. S. Mason, and F. H. Marshall, "Progress in structure based drug design for G protein-coupled receptors," *Journal of Medicinal Chemistry*, vol. 54, no. 13, pp. 4283–4311, 2011.
- [4] A. Bilkei-Gorzo, O. M. Abo-Salem, A. M. Hayallah, K. Michel, C. E. Müller, and A. Zimmer, "Adenosine receptor subtype-selective antagonists in inflammation and hyperalgesia," *Naunyn-Schmiedeberg's Archives of Pharmacology*, vol. 377, no. 1, pp. 65–76, 2008.
- [5] S. Redenti, A. Cianchetta, G. Pastorin et al., "Pyrazolo[4,3-e][1,2,4]triazolo[1,5-c]pyrimidines and structurally simplified analogs. Chemistry and SAR profile as adenosine receptor antagonists," *Current Topics in Medicinal Chemistry*, vol. 16, no. 28, pp. 3224–3257, 2016.
- [6] A. El Maatougui, J. Azuaje, M. González-Gómez et al., "Discovery of potent and highly selective A2B adenosine receptor antagonist chemotypes," *Journal of Medicinal Chemistry*, vol. 59, no. 5, pp. 1967–1983, 2016.
- [7] M. de Lera Ruiz, Y. H. Lim, and J. Zheng, "Adenosine A<sub>2A</sub> receptor as a drug discovery target," *Journal of Medicinal Chemistry*, vol. 57, no. 9, pp. 3623–3650, 2014.
- [8] G. Yuan, N. G. Gedeon, T. C. Jenkins, and G. B. Jones, "Novel approaches for targeting the adenosine A<sub>2A</sub> receptor," *Expert Opinion on Drug Discovery*, vol. 10, no. 1, pp. 63–80, 2015.
- [9] G. Yuan and G. B. Jones, "Towards next generation adenosine A<sub>2A</sub> receptor antagonists," *Current Medicinal Chemistry*, vol. 21, p. 3918, 2014.
- [10] A. Chouker, M. Thiel, D. Lukashev et al., "Critical role of hypoxia and A<sub>2A</sub> adenosine receptors in liver tissue-protecting physiological anti-inflammatory pathway," *Molecular Medicine*, vol. 14, p. 116, 2008.
- [11] D. Lukashev, A. Ohta, and M. Sitkovsky, "Hypoxia-dependent anti-inflammatory pathways in protection of cancerous tissues," *Cancer and Metastasis Reviews*, vol. 26, no. 2, pp. 273–279, 2007.
- [12] D. Lukashev, M. Sitkovsky, and A. Ohta, "From 'Hellstrom paradox' to anti-adenosinergic cancer immunotherapy," *Purinergic Signalling*, vol. 3, no. 1-2, pp. 129–134, 2007.
- [13] M. Sitkovsky, D. Lukashev, S. Deaglio, K. Dwyer, S. C. Robson, and A. Ohta, "Adenosine A<sub>2A</sub> receptor antagonists: blockade of adenosinergic effects and T regulatory cells," *British Journal of Pharmacology*, vol. 153, no. 1, pp. S457–S464, 2008.
- [14] M. V. Sitkovsky, "T regulatory cells: hypoxia-adenosinergic suppression and re-direction of the immune response," *Trends in Immunology*, vol. 30, no. 3, pp. 102–108, 2009.
- [15] M. V. Sitkovsky, J. Kjaergaard, D. Lukashev, and A. Ohta, "Hypoxia-adenosinergic immunosuppression: Tumor protection by T regulatory cells and cancerous tissue hypoxia," *Clinical Cancer Research*, vol. 14, no. 19, pp. 5947–5952, 2008.
- [16] R. Thomas, J. Lee, V. Chevalier et al., "Design and evaluation of xanthine based adenosine receptor antagonists: Potential hypoxia targeted immunotherapies," *Bioorganic & Medicinal Chemistry*, vol. 21, no. 23, pp. 7453–7464, 2013.
- [17] A. Ohta and M. Sitkovsky, "Role of G-protein-coupled adenosine receptors in downregulation of inflammation and protection from tissue damage," *Nature*, vol. 414, no. 6866, pp. 916–920, 2001.
- [18] R. A. Hodgson, R. Bertorelli, G. B. Varty et al., "Characterization of the potent and highly selective A<sub>2A</sub> receptor antagonists preladenant and SCH 412348 [7-[2-[4-(2,4-difluorophenyl)-1-piperazinyl]ethyl]-2-(2-furanyl)-7hpyrazolo[4,3-e][1,2,4]triazolo[1,5-c]pyrimidin-5-amine in rodent models of movement disorders and depression," *The Journal of Pharmacology and Experimental Therapeutics*, vol. 330, no. 1, pp. 294–303, 2009.
- [19] R. A. Hauser, F. Stocchi, O. Rascol et al., "Preladenant as an adjunctive therapy with levodopa in Parkinson disease: two randomized clinical trials and lessons learned," *JAMA Neurology*, vol. 72, no. 12, pp. 1491–1500, 2015.
- [20] T. T. Wager, X. Hou, P. R. Verhoest, and A. Villalobos, *ACS Chem. Neurosci*, vol. 1, p. 435, 2010.
- [21] V.-P. Jaakola, M. T. Griffith, M. A. Hanson et al., "The 2.6 angstrom crystal structure of a human A<sub>2A</sub> adenosine receptor bound to an antagonist," *Science*, vol. 322, no. 5905, pp. 1211–1217, 2008.
- [22] H. Piirainen, Y. Ashok, R. T. Nanekar, and V.-P. Jaakola, "Structural features of adenosine receptors: from crystal to function," *Biochimica et Biophysica Acta (BBA) - Biomembranes*, vol. 1808, no. 5, pp. 1233–1244, 2011.
- [23] R. A. Friesner, R. B. Murphy, M. P. Repasky et al., "Extra precision glide: Docking and scoring incorporating a model of hydrophobic enclosure for protein-ligand complexes," *Journal of Medicinal Chemistry*, vol. 49, no. 21, pp. 6177–6196, 2006.
- [24] R. A. Friesner, J. L. Banks, R. B. Murphy et al., "Glide: a new approach for rapid, accurate docking and scoring. 1. Method and assessment of docking accuracy," *Journal of Medicinal Chemistry*, vol. 47, no. 7, pp. 1739–1749, 2004.
- [25] T. A. Halgren, R. B. Murphy, R. A. Friesner et al., "Glide: a new approach for rapid, accurate docking and scoring. 2. Enrichment factors in database screening," *Journal of Medicinal Chemistry*, vol. 47, no. 7, pp. 1750–1759, 2004.
- [26] D. Shivakumar, J. Williams, Y. Wu, W. Damm, J. Shelley, and W. Sherman, "Prediction of absolute solvation free energies using molecular dynamics free energy perturbation and the opls force field," *Journal of Chemical Theory and Computation*, vol. 6, no. 5, pp. 1509–1519, 2010.
- [27] R. A. Hauser, C. W. Olanow, K. D. Kieburtz et al., "Tozadenant (SYN115) in patients with Parkinson's disease who have motor fluctuations on levodopa: A phase 2b, double-blind, randomised trial," *The Lancet Neurology*, vol. 13, no. 8, pp. 767–776, 2014.

- [28] Biotie Therapies: Biotie announces start of tozadenant Phase 3 Study in Parkinson's disease. Press Release, July 21, 2015.
- [29] P. Bandyopadhyay, S. K. Agrawal, M. Sathe, P. Sharma, and M. P. Kaushik, "A facile and rapid one-step synthesis of 8-substituted xanthine derivatives via tandem ring closure at room temperature," *Tetrahedron*, vol. 68, no. 20, pp. 3822–3827, 2012.
- [30] S. C. Kuo, L. T. Tran, and P. Zhang, WO054245 A3.
- [31] A. Flohr, J. L. Moreau, S. Poli, C. Riemer, and L. Steward, US20050261289 A1.
- [32] E. Marom, M. Mizhiritskii, and S. Rubnov, WO2012127472 A1.
- [33] C. Vala, T. J. Morley, X. Zhang et al., "Synthesis and in vivo Evaluation of Fluorine-18 and Iodine-123 Pyrazolo[4,3-e]-1,2,4-triazolo[1,5-c]pyrimidine Derivatives as PET and SPECT Radiotracers for Mapping A2A Receptors," *ChemMedChem*, pp. 1936–1943, 2016.
- [34] M. Cui, M. Ono, H. Kimura et al., "Novel 18F-labeled benzoxazole derivatives as potential positron emission tomography probes for imaging of cerebral  $\beta$ -amyloid plaques in alzheimers disease," *Journal of Medicinal Chemistry*, vol. 55, no. 21, pp. 9136–9145, 2012.
- [35] A. Coop and K. C. Rice, US6395900 B1.
- [36] A. Ohta, E. Gorelik, S. J. Prasad et al., "A2A adenosine receptor protects tumors from antitumor T cells," *Proceedings of the National Academy of Sciences of the United States of America*, vol. 103, no. 35, pp. 13132–13137, 2006.
- [37] S. Apasov, J. F. Chen, P. Smith, and M. Sitkovsky, "A2A receptor dependent and A2A receptor independent effects of extracellular adenosine on murine thymocytes in conditions of adenosine deaminase deficiency," *Blood*, vol. 95, 3859 pages, 2000.
- [38] O. Barret, J. Hannestad, C. Vala et al., "Characterization in humans of  $^{18}\text{F}$ -MNI-444, a PET radiotracer for brain adenosine 2A receptors," *Journal of Nuclear Medicine*, vol. 56, no. 4, pp. 586–591, 2015.
- [39] E. Krieger and G. Vriend, "YASARA view—molecular graphics for all devices—from smartphones to workstations," *Bioinformatics*, vol. 30, no. 20, pp. 2981–2982, 2014.



